PCCP

Accepted Manuscript

ROYAL SOCIETY OF CHEMISTRY

www.rsc.org/pccp

Journal Name

RSCPublishing

ARTICLE

Charge Density Study of the π–Delocalization and Intermolecular Interactions

Cite this: DOI: 10.1039/x0xx00000x

L.-C. Wu,[a] W.-C. Chung,[a] C.-C. Wang,*[b] G.-H. Lee,[c] S.-I Lu,[b] and Y. Wang*[a],

Received ooth January 2012,
Accepted ooth January 2012

DOI: 10.1039/x0xx00000x

www.rsc.org/

The compound trans-4,4'-azo-1,2,4-triazole (**atrz**) is a planar molecule with two planar triazole rings bridged by an *azo* group. The molecule is a good donor ligand and has an interesting π–delocalized character. In addition, intermolecular interactions in the crystalline state through π–π stacking are found between triazole rings with a very short inter-planar distance of 3.17 Å. The electron density distribution is obtained both from high resolution X-ray diffraction data at 100 K and from a density functional theory (DFT) calculation using ωB97X-D functional. Bond characterization is made in terms of charge density distribution and the associated topological properties. Laplacian distribution around each atom reveals the shape of the valence-shell charge concentration and demonstrates a sp^2 hybrid orbital shape of each atom in the molecule. The π–delocalization of the planar molecule is further illustrated by the Fermi-hole distribution. The weak intermolecular π–π interactions and hydrogen bonds are further illustrated through Hirshfeld surface. The energies of weak intermolecular π–π interactions and hydrogen bonds have been calculated through ωB97X-D/6-311++G(3df,2p) at experimental geometry.

Introduction

It is well known that intermolecular interactions play crucial role in the packing of molecules in crystalline materials.[1] Topological analysis of detail electron density distribution of organic, organometallic, inorganic, or ionic solid in crystalline state is now a mature and highly productive field.[2, 3] The experimental charge density based on high resolution X-ray diffraction data has been employed successfully to understand the bonding and properties of molecular systems during the last few decades.[4, 5, 6, 7, 8] There are electron density studies of crystals which consist of strong and weak intermolecular interactions, such as hydrogen bonding. Many studies have applied the 'Atoms in Molecules–A Quantum Theory (QTAIM)'[9] approach to both theoretical and experimental electron densities.[5, 6, 7, 10] In this approach, the gradient vector field of the electron density, $\nabla\rho(r)$, and the Laplacian of the electron density, $\nabla^2\rho(r)$ are calculated. Bond characterizations are expressed through $\rho(r)$, $\nabla\rho(r)$ and $\nabla^2\rho(r)$ associated with bond critical point (BCP); a few excellent review articles[3] have been published in this respect. Strong hydrogen bonds,[11, 12] for example, the O–H···O, N–H···O, and N–H···N, have been carefully studied to elucidate the nature of these interactions.[4, 12] The importance of some weak hydrogen bonds such as C–H···O, C–H···N, N–H···π, C–H···π, H···H etc. have also been explored during the last decade.[13, 14] Their significant roles are recognized in the stabilization of supramolecular architecture, crystal packing and molecular recognition.[15, 16]

Trans-4,4'-azo-1,2,4-triazole (**atrz**) is a nitrogen-rich compound with a planar conformation containing a unique N–N=N–N linkage between two planar triazole rings. Synthesis, structural characterization and physical properties have been described in the literature.[17, 18] The most striking feature of **atrz** molecule is its 3D supramolecular network constructed via intermolecular π–π interactions between triazole rings and two C–H···N hydrogen bonds. Such stacking force is worth of investigating to shed lights on the origin of molecular packing in the crystal. In this work, we carried out a detailed analysis of experimental and theoretical electron density distributions of **atrz** molecule on the purpose of characterizing the intra- and inter-molecular interactions. The role of π–π interaction in the crystal packing is under our special interest.

Results and Discussion

Structure Description and the Multipole Model

Molecular structure of **atrz** with atomic labelling and local coordinates is depicted in Figure 1. The molecule is in C_i symmetry with the center of inversion located at the midpoint along N4–N4A bond. The molecular structure at 100 K is the same as that of room temperature.[18] However, the agreement indices (R-factors) are high with significant residuals located at the bonding regions shown in Figure 2(a). To improve the model refinement, a multipole model[19] (MM) based on spherical harmonic functions is employed. The success of the MM is clearly demonstrated in its significant improvement in the agreement indices (a reduction of R_{2w} from 0.088 to 0.033 using 4086 observed reflections, (Table 1), as well as the essentially featureless residual density map after the refinement as depicted in Figure 2(b). The progressive improvement through the

MM refinement is listed in supporting information of Table S2. The crystal packing is shown in Figure 3(a), where the planar molecules are nicely stacked with all the molecules parallel to one another; the unique zigzag chain-like stacking via π–π interactions between adjacent triazole rings with interplanar distance of 3.17 Å is displayed in Figure 3(b). The 3D supramolecular architecture is further enhanced by two weak intermolecular C–H···N hydrogen bonds with distances of 3.252 Å for C1–H1···$N1_i$, and 3.343 Å for C2–H2···$N2_{ii}$ as dashed line shown in Figure 3(a). The detail descriptions of π–π interaction and hydrogen bonding are provided in supporting information on Table S4 and S5.

Table 1. Agreement indices of various refinements for **atrz**.

N_{ref}[a]: 4086	N_v [a]	N_{ref}/N_v	R_1[b]	R_{1w}[b]	R_2[b]	R_{2w}[b]	GOF[b]
Spherical	54	75.67	0.031	0.044	0.057	0.088	5.318
Octapole	180	25.70	0.016	0.016	0.030	0.033	2.001

[a] N_{ref}: number of reflections. N_v: number of variables.
[b] $R_1=\Sigma|F_o-F_c|/\Sigma|F_o|$; $R_{1w}=(\Sigma|w|F_o-F_c|^2|/\Sigma|wF_o^2|)^{1/2}$; $R_2=[\Sigma|F_o^2-F_c^2|/\Sigma(F_o^2)]$; $R_{2w}=\{\Sigma|w(F_o^2-F_c^2)^2|/\Sigma|w(F_o^2)^2|]\}^{1/2}$; GOF=$[\Sigma w|F_o-F_c|^2/(N_{ref}-N_v)]^{1/2}$, $w = 1/[\sigma(F_o^2)]$

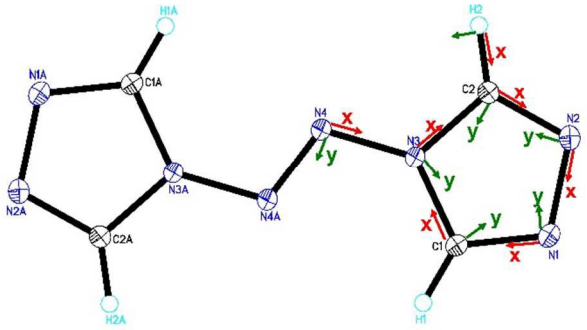

Figure 1 Molecular structure of trans-4,4'-azo-1,2,4-triazole and local coordinates of each atom. The ORTEP is drawn with 50% probability in thermal ellipsoids at 100K. A: 1-x, 1-y, -z.

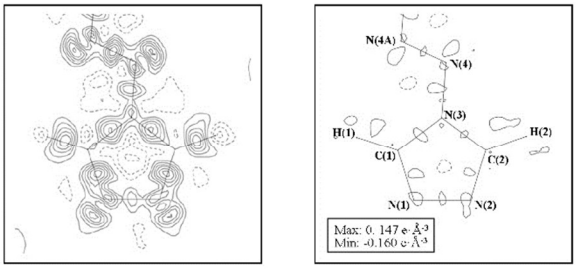

Figure 2. Residual density maps, $\Delta\rho_{residual}$ (F_{obs} - F_{model}). after the (a) spherical model; (b) multipole model at the plane of 1,2,4,-triazole ring. Contour interval is 0.1 eÅ^{-3}; solid line is positive and dashed line negative.

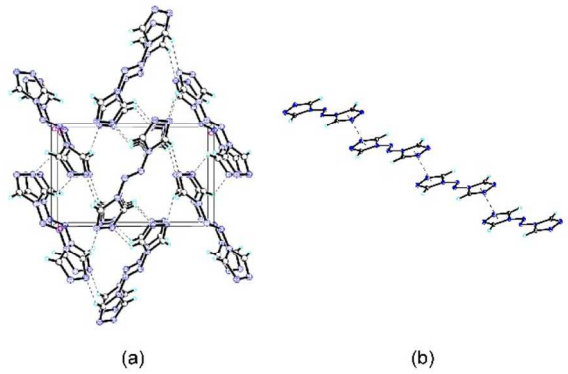

Figure 3. Packing diagram of **atrz** molecules in crystal with two weak C–H···N intermolecular hydrogen bonding interactions (dashed lines). (b) The zigzag-like chain of the π–π stacking interaction.

Deformation Density

Deformation density is expressed as the difference in electron density between the MM and the independent spherical atom model (IAM). Deformation density maps of the unique part of **atrz** molecule are depicted in Figure 4. Experiment and theory give very similar result on the chemical bonding region, though significant differences are observed near nuclear regions probably due to the differences of radial function,[20] which are often observed in such studies.[14, 16, 21, 22] Deformation density is found in every bonding region of the N–N, C–N and C–H bonds as expected; so as in every lone pair region of nitrogen atoms (N1, N2 and N4). It is noteworthy that the experimental deformation density maxima along the N–N bond is in the order of 0.1, 0.3 and 0.5 eÅ^{-3}, corresponding to the bond lengths of N1–N2 (1.4058(5) Å), N3–N4 (1.3715(3) Å) and N4–N4A (1.2458(5) Å). The same trend is found along C–N bonds, where the density maximum is higher along C1–N1, C2–N2 bonds (average bond length 1.304 Å) than those along C1–N3, C2–N3 bonds (average bond length 1.372 Å).

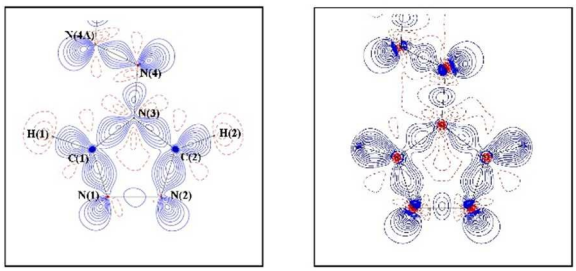

Figure 4. Deformation density map, $\Delta\rho_{M-A}$, from (a) MM and (b) DFT at the plane of 1,2,4,-triazole ring. Contour interval is 0.1 eÅ^{-3}; solid line (blue) is positive and dashed line (red) negative.

Laplacian Distribution

Laplacian of electron density is obtained from the second derivative of the total electron density; it provides the local charge concentration (LCC) and local charge depletion (LCD). The Laplacian distribution of the **atrz** molecule from experiment and theory are in good agreement, as depicted in Figure 5. The LCCs of each atom display in a triangle shape around each C or N nucleus, which reflect the valence shell charge concentration (VSCC) of the

carbon or nitrogen atom is in its sp^2 hybrid configuration. Based on the QTAIM,[9] the gradient field of the electron density at the molecular plane together with the BCPs and bond paths are illustrated in Figure 6. The projected atomic basin correlates well with its bonding environment; again the basins of carbon and nitrogen atoms at the molecular plane are all in triangular shape, which further reinforces the feature of sp^2 hybrids of these atoms. The BCPs are at the midpoint along N–N bonds; but slightly towards the C atom along C–N bonds, which are as expected from the relative electronegativity.

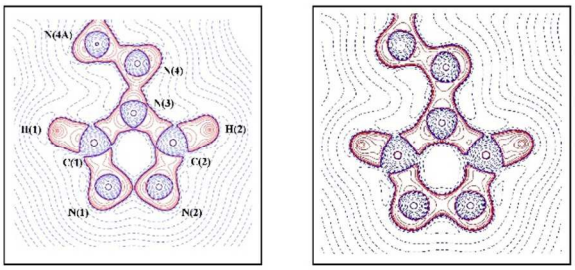

Figure 5. Laplacian map, $\nabla^2\rho(r)$, from (a) MM and (b) DFT at the same plane as in Figure 4; contours are in steps of $\pm 2^m 10^n$ (m = 1 to 3; n = -3 to +3); dash line (blue) is positive and solid lines (red) negative.

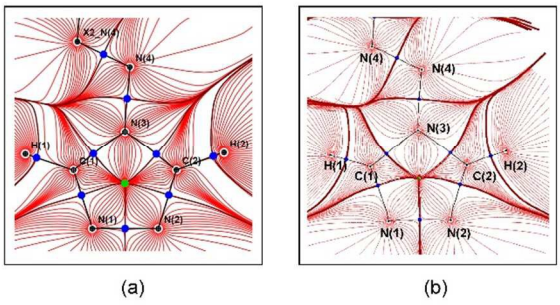

Figure 6. The gradient field of the electron density ($\nabla\rho$) at the molecular plane: from (a) MM (b) DFT model; atoms are shown as black dots, BCPs are in blue dots, and RCP (ring critical point) is in green dot; the zero flux surfaces, $n\cdot\nabla\rho = 0$, are drawn as brown lines; bond paths are in black lines.

Topological Properties

Topological properties associated with the BCPs both from MM model and from DFT calculation are listed in Table 2. It is noteworthy that all the chemical bonds have a high electron density value (ρ_{BCP} > 2 eÅ^{-3}) and a large negative Laplacian, $\nabla^2\rho_{BCP}$, at the BCP, representing a typical shared interaction, i.e. covalent character (with the exception on N1-N2 bond, due to its low values of λ_1 and λ_2; which is consistent with the Laplacian distribution shown in Figure 5a). It is important to note that among N–N bonds; the increasing ρ_{BCP} values (MM and DFT) for the N1–N2 bond (2.07 and 2.21 eÅ^{-3}), N3–N4 bond (2.33 and 2.40 eÅ^{-3}), and N4–N4A bond (3.21 and 3.25) are in accord with the decreasing bond lengths of N1–N2 (1.4058(5) Å), N3–N4 (1.3715(3) Å) and N4–N4A (1.2458(5) Å) as shown in Table 2. Such correlation indicates that the ρ_{BCP} value can be used as an indicator of the bond strength in a more quantitative way, which has been recognized elsewhere.[9] Here the shortest N4–N4A bond is in double bond character with a ρ_{BCP} value as high as 3.2 eÅ^{-3}; where the other two bonds are in partial double-bond character, but N3–N4 is stronger than N1–N2. In addition, the bond strengths of different chemical bonds can be compared based on the ρ_{BCP} values, which is not possible to achieve based on the bond distances. For example, the N1–C1 and N2–C2 bonds are slightly stronger than that of N3–N4, but much weaker than that of N4–N4A. Furthermore, N3–C1 and N3–C2 bonds have similar bond strength to N1–N2. It does help to understand the bonding type in a molecule.

Table 2. Topological properties associated with BCP: 1st line from experimental MM and 2nd line (*Italic*) from DFT calculation.

Bond	d_1[a]	ρ_{BCP}	$\nabla^2\rho_{BCP}$	$\lvert\lambda_1\rvert/\lambda_3$[b]	V_{BCP}[c]	H_{BCP}[d]
Bond distance	(Å)	(eÅ^{-3})	(eÅ^{-5})		(HÅ^{-3})	(HÅ^{-3})
N1–N2	0.701	2.07	0.39	0.50	-4.70	-2.33
1.4058(5)	*0.704*	*2.21*	*-12.28*	*0.80*	*-3.10*	*-1.98*
N3–N4	0.707	2.33	-5.60	0.62	-5.28	-2.84
1.3715(3)	*0.697*	*2.40*	*-16.38*	*0.90*	*-3.45*	*-2.30*
N4–N4A	0.623	3.21	-18.71	0.80	-8.21	-4.76
1.2458(5)	*0.591*	*3.25*	*-29.45*	*1.17*	*-6.13*	*-4.10*
N1–C1	0.745	2.66	-29.66	1.85	-5.01	-3.54
1.3046(4)	*0.803*	*2.58*	*-29.62*	*2.20*	*-5.70*	*-3.89*
N2–C2	0.744	2.66	-28.88	1.80	-5.02	-3.52
1.3041(4)	*0.800*	*2.58*	*-30.03*	*2.23*	*-5.67*	*-3.89*
N3–C1	0.825	2.17	-22.43	1.80	-3.81	-2.69
1.3741(4)	*0.879*	*2.06*	*-18.67*	*1.49*	*-4.68*	*-2.99*
N3–C2	0.827	2.21	-24.31	1.96	-3.87	-2.78
1.3691(4)	*0.880*	*2.10*	*-19.38*	*1.47*	*-4.86*	*-3.11*

[a] d_1: distance of BCP to the first atom. [b] λ_1, λ_3: Hessian Eigenvalues; [c]$V_{BCP.}$: potential energy density; [d] H_{BCP}: total energy density.

Fermi-Hole Distribution

Bond delocalization is best described by the Fermi-hole function.[9, 23] It is demonstrated that all physical measures of the electron localization or delocalization can be illustrated by the corresponding localization or delocalization of the Fermi hole distribution based on the Pauli exclusion principle, such as M–L multiple bond[6] and metal–metal multiple bond[7, 24] The Fermi hole distribution of **atrz** is displayed in Figure 7 with the reference electron located 0.5 a.u. above the plane of the molecule at various atomic sites. It is noteworthy that the π delocalization of the **atrz** molecule is limited to each triazole ring itself. The density spread in space covers the whole triazole ring when the reference electron is located above any ring atom; however the density spreads only over the central four nitrogen part, (N3–N4=N4A–N3A) when the reference electron is located above any of these nitrogen atoms (Figure 7(f)) of the *azo* group. This implies that the π-delocalization of the **atrz** molecule exists only on each triazole ring, which is separated by a localized *azo* N-N double bond; even though the molecule is perfectly planar.

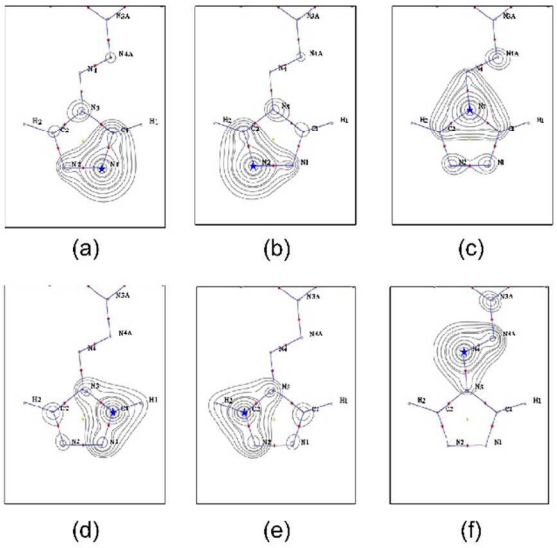

Figure 7. Fermi-hole distributions based on DFT calculation with the reference electron (★) placed 0.5 au above the molecular plane at various atomic sites: (a) N1, (b) N2, (c) N3, (d) C1, (e) C2, (f) N4.

Molecular Orbital Analysis

The molecular orbital (MO) analysis is performed by using ωB97X-D calculation. Since the π-delocalization is particularly interesting in this planar molecule, the p_π orbitals are analysed. A total of 12 π MOs is depicted in Figure S1, seven of them are occupied π-orbitals below the highest occupied MO (HOMO, #42), which is an in-plane σ-bond, the other five are unoccupied π*-orbitals including the lowest unoccupied MO (LUMO, #43). It is clear from the seven occupied π-orbitals (MO #26, 30, 33, 35, 38, 39 and 40) that the π-delocalization mainly located in the five-membered triazole ring with a localized *azo* double bond. Also the p_π overlap between N3 and N4 is small in all occupied π-MOs except at the lowest energy π-orbital (MO #26) mainly contributed from the central four N atoms, N3-N4-N4A-N3A. This again is consistent with the observation from the Fermi hole distribution.

Molecular Electrostatic Potential

The molecular electrostatic potential (MEP) derived from the MM and DFT total electron density is depicted in Figure 8. Experimental and theoretical MEPs appear an electron donor site on the surface near N1–N2 bonds and an electron acceptor site on the surface near the H atoms. Accordingly, this explains well on the C–H···N intermolecular interaction displayed in the crystal packing (Figure 8(a)).

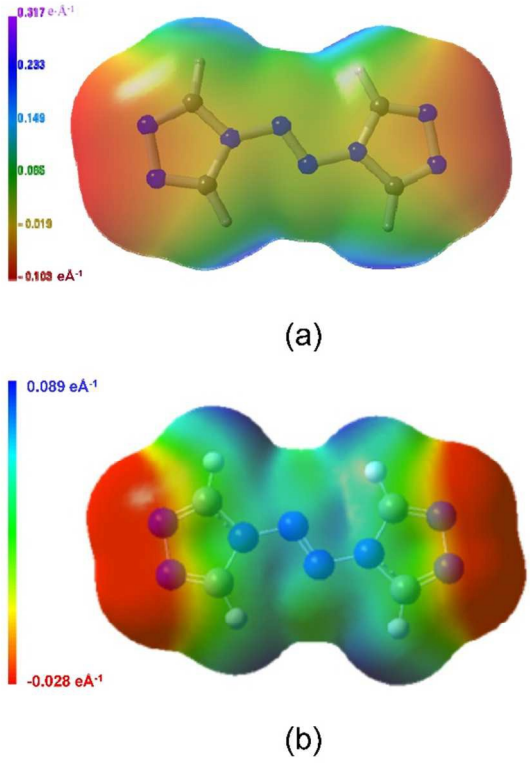

Figure 8. Molecular electrostatic potential (MEP) of **atrz** molecule based on (a) MM and (b) DFT.

Hydrogen Bonding

The existence of an intermolecular hydrogen bonding through C–H···N is indeed observed in the crystal between the neighboring molecules, which is evidenced by the experimental charge density study. The experimental bond critical point is located and the corresponding bond paths are traced as shown in Figure 9 and 10. Due to the symmetry, the C1–H1···N1$_i$ hydrogen bond is formed in pairs. In fact, it is clearly indicative from the corresponding deformation density and Laplacian distribution that one of LCC, i.e. the lone pairs of N, is directed toward the H atom of the neighboring molecule. Nevertheless, unlike the chemical bond, the bond path is often curved and not easy to locate, especially the weak ones. The topological properties listed in Table 3 give a very small value of ρ_{BCP} (0.05 eÅ^{-3}), a small positive $\nabla^2\rho_{BCP}$ (~ 0.9 eÅ^{-5}), and a close to zero value of total energy density,[25] H_{BCP}, which are similar to those of other organic molecules.[13, 14]

The hydrogen bond energies (E_{HB}) estimated from wB97X-D/6-311++G(3df,2p) on a dimer are 3.62 and 3.61 kcal/mol for C1–H1···N1$_i$ and C2–H2···N2$_{ii}$, respectively; which is quite comparable to that of 3.35 kcal/mol for 3,4-diamino-1,2,4-triazole (DAT).[16]

Table 3. Experimental topological properties and DFT calculated energies of hydrogen bond and π···π interactions of **atrz**.

	D[a] (Å)	R_{12}[a] (Å)	d_1[a] (Å)	ρ_{BCP} (eÅ^{-3})	$\nabla^2\rho_{BCP}$ (eÅ^{-5})	V_{BCP} (HÅ^{-3})	H_{BCP} (HÅ^{-3})	$E_{interaction}$ (kcal/mol)
H1···N1$_i$[b]	2.45	2.50	0.99	0.05	0.82	-0.03	0.01	3.62[c]
H2···N2$_{ii}$[b]	2.39	2.40	0.92	0.06	0.94	-0.04	0.01	3.61[c]
N1···N3$_{iii}$[b]	3.20	3.26	1.59	0.05	0.64	-0.02	0.01	8.12[d]
N2···C1$_{iii}$	3.27	3.30	1.68	0.05	0.54	-0.02	0.01	

[a] D: distance between atoms. R_{12}: sum of path lengths between BCP and atom 1 (first atom) and 2 (second atom). d_1: distance from BCP to the atom 1. [b] Symmetry operations: i=1-x, 1-y, -z; ii=-0.5-x, -0.5+y, 0.5-z. iii=-x, 1-y, -z. [c] Hydrogen bond. [d] π···π interaction.

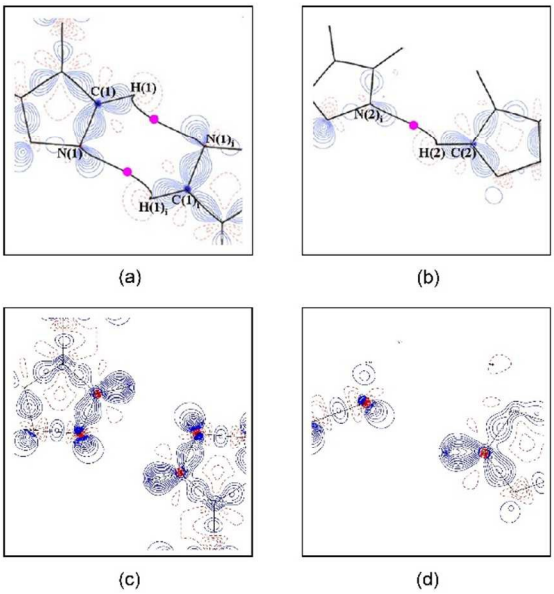

Figure 9. Deformation density of hydrogen bonding: (a) C1–H1···N1 (b) C2–H2···N2 from MM model; (c, d) are the corresponding maps from DFT. BCPs and bond paths are indicated in (a) and (b). The contour levels are as in Figure 4.

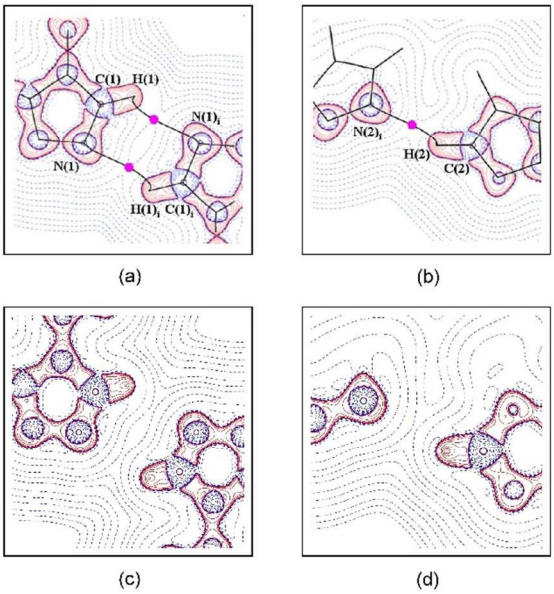

Figure 10. Laplacian distribution of the hydrogen bonds: (a) C1–H1···N1 (b) C2–H2···N2 from MM model; (c) and (d) are the corresponding ones from DFT. BCPs and bond paths are drawn in (a) and (b). The contours are as in Figure 5.

π···π Interaction

In addition, the molecules are stacked in parallel in the crystal as indicated in Figure 3, with a very short inter-planar distance (3.17 Å), which is in a perfect condition to accommodate π···π interactions between the neighboring molecular planes shown in Figure 11(a). Based on the Fermi hole distribution, the π-delocalization is allocated mainly on the five-membered ring. The π···π interaction is further evidenced with four BCPs (along N1···N3$_{iii}$ and N2···C1$_{iii}$) and corresponding bond paths allocated as depicted in Figure 11(b) with the topological properties listed in Table 3; one has to note that the ρ_{BCP} values are very low (0.05 eÅ^{-3}) and the associate bond paths are curved. The experimental charge density analysis of π···π interaction is not often presented.[16, 22] However theoretical calculations on benzene molecules[26, 27] and other systems[28] have been reported. The importance of π···π interaction in some bio-systems is addressed recently.[27, 29]According to the classification of intermolecular interaction based on topological properties,[11] there are shared shell ($\nabla^2\rho_{BCP} < 0$, $H_{BCP} < 0$, $|V_{BCP}|/G_{BCP} > 2$), close shell ($\nabla^2\rho_{BCP} > 0$, $H_{BCP} < 0$, $1 < |V_{BCP}|/G_{BCP} < 2$) and pure close shell ($\nabla^2\rho_{BCP} > 0$, $H_{BCP} > 0$, $|V_{BCP}|/G_{BCP} < 1$) interactions. Accordingly, these two types of intermolecular interactions (hydrogen bonding and π-π interaction) can be classified as pure close shell interaction. The result is similar to that of DAT and its 5-methyl derivative.[16]

Waller et al.[30] proposed a linear relationship between binding energy, ΔE and the sum of ρ_{BCP} values of intermolecular interactions to estimate π–π interaction energy for benzene, pyridine, and DNA/RNA bases compounds. The binding energy of **atrz** thus estimated is 5.15 kcal/mol, which is about the same as those of adenine/benzene (4.60 kcal/mol) and guanine/benzene (5.61 kcal/mol) complexes but twice bigger than pure benzene (~2.31 kcal/mol) or pyridine (2.88 kcal/mol) compounds.[30] The calculated one based on wB97X-D is 8.12 kcal/mol.

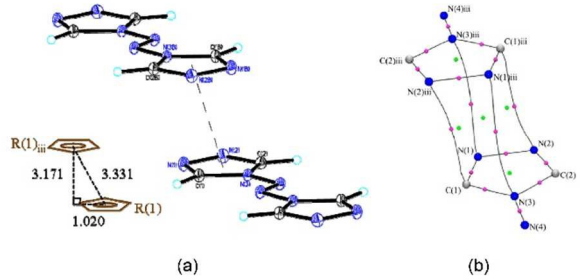

Figure 11. (a) The π–π stacking with the inter-planar distance of 3.17Å. (b) Bond paths (solid black lines) and BCPs (pink dots) are indicated along N1···N3$_{iii}$ and N2···C1$_{iii}$ interactions (*iii* = -x, 1-y, -z). Ring critical points (green dots) are also marked.

Hirshfeld Surface

The Hirshfeld surface of **atrz** molecule is shown in Figure 12(a), where the N···H–C hydrogen bonds and the π···π interactions are manifested in a donor/acceptor character between **atrz** molecules. The d_{norm} map[31, 32] depicted in Figure 12(b), highlights the locations of these hydrogen bonding and π–π interactions (marked in red circles).

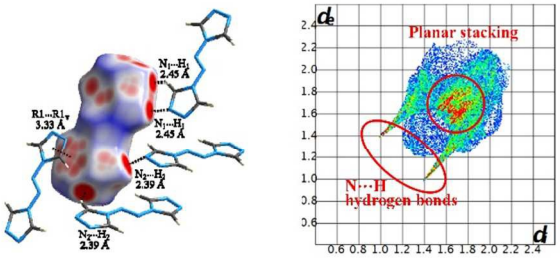

Figure 12. (a) Hirshfeld surface of an **atrz** molecule mapped with d_{norm}; white color describes the distance of two atoms is equals to the sum of van der Waals radius of two atoms; red and blue is shorter and larger than the sum respectively. (b) Fingerprint plot for the single molecule. Features characteristic of key intermolecular contacts are circled in red.

Experimental

Synthesis of trans-4,4'-azo-1,2,4-triazole

Trans-4,4'-azo-1,2,4-triazole was synthesized via a direct mixing of $KBrO_3$ and 4-amino-4H-1,2,4-triazole in 50 mL water and stirred for ten minutes. HCl (6 mL) was then slowly added into the solution while stirring until the color of the solution turned from pale-yellow to orange. The yellow precipitates were then filtered out and washed with de-ionized water. Re-crystallization from aqua solution yielded rod-shape yellow crystals.

Crystallographic Data Collection and Refinement

The high-resolution single-crystal X-ray diffraction data of **atrz** were measured on a Nonius Kappa CCD diffractometer at 100(2) K using Mo K_α radiation (wavelength of 0.71073 Å). A light-yellow single crystal with dimensions of 0.24 × 0.20 × 0.20 mm was mounted on a goniometer head under the liquid nitrogen stream and was placed at 4.00 cm away from the detector. Low order (2.0°~27.5°) and high order (15.5°~58.52°) data sets were collected with a scan angle of 0.5°/frame and exposure times of 10 and 200 s, respectively. The highest resolution ($\sin\theta/\lambda$) reached 1.2 $Å^{-1}$. Data collection and relative intensity integration were performed using the software DENZO.[33] Two data sets were merged and scaled according to the reflections in the overlapping region after applying the absorption correction based on the face measurements using SADABS.[34] All hydrogen atoms of the **atrz** molecule were generated according to the ideal geometry of the connected atoms assuming sp^2 hybridization and refined using riding model. Full-matrix least-squares refinement on F^2 was applied using observed reflections ($I > 2\ \sigma(I)$). All processes were carried out using the program SHELXL.[35] Details on the data collection and refinements at 100 K are given in supporting information (Table S1). Complete crystallographic data are deposited in CCDC-936888. The data can be obtained free of charge at www.ccdc.cam.ac.uk/conts/retrieving.html or from CCDC deposit@ccdc.cam.ac.uk].

Multipole Model Refinement

A multipole model (MM) refinement was carried out based on the Hansen and Coppens model[19] in which the atomic electron density is described as

$$\rho_{atom}(r) = \mathrm{P}_c\rho_{core}(r) + P_{val}\kappa^3\rho_{val}(\kappa r) + \sum_{l=0}^{l_{max}}\kappa'^3\ R_l(\kappa' r)\sum_{m=0}^{l}P_{lm\pm}d_{lm\pm}(\theta,\phi)$$

$$\mathrm{R}_l(\mathrm{r}) = \kappa'^3\frac{\zeta^{n_l+3}}{(n_l+2)!}(\kappa' r)^{n_l}\,e^{-\kappa'\zeta r}$$

The first two terms are the spherical part of atomic electron density; the third one describes the nonspherical part of the electron density, which is expressed as the sum of multipole terms using the real part of spherical harmonic functions (Y_{lmp}); $R_l(r)$ is the radial function; both κ and κ' serve as the expansion-contraction factor of the radial distribution. P_c and P_{val} are the populations of the core and valence electrons, respectively; P_{lm} is the coefficient of multipole term; all P_{lm} parameters and P_{val}, κ, κ' are obtained through the MM refinements using the XD2006[36] program. Clementi and Raimondi wave function[37] and their single-ξ Slater-type functions[38] were used. Spherical atomic scattering amplitudes were taken from *International Table for X-ray Crystallography*.[39] The atomic structural parameters including positional and thermal displacements were first refined using high-order data ($\sin\theta/\lambda > 0.7$); then multipole terms were included up to octapole for N and C atoms, and up to dipole for H atoms. During the refinement, H atoms are moved along the C–H vectors to make a C–H distance of 1.087 Å.[40] The values of n_l are (2 2 3) for N and C atoms and (1 2) for H atoms, respectively. Topological analyses were applied based on Bader's QTAIM.[9] The experimental total electron density is derived according to the MM. Topological properties associated with the bond critical point (BCP) and Laplacian distributions were obtained by using the XD2006 program.[36] The theoretical deformation density and Laplacian distributions were derived from XDPROP.[41] Theoretical topological properties at BCPs and Fermi hole distributions were derived from XAIM program.[42]

Computational Details

Gaussian09 suite of programs[43] was used to perform electron density and energy computations based on the experimental geometry of **atrz** at 100 K. To include non-covalent interaction (for examples, π–π interaction and hydrogen bonding) appropriately, ωB97X-D exchange-correlation (XC) functional[44] with the 6-311++G(3df,2p) basis set was used. The basis set superposition errors (BSSE) were also taken into consideration for π–π interaction and hydrogen bonding of interest. Hirshfeld surface analysis[31, 45] for the intermolecular interactions was carried out using the program *CrystalExplorer*.[46]

Conclusions

A deep understanding of π-delocalization and the intermolecular interactions of **atrz** molecules in crystal has been probed by topological analysis of electron density distribution. Bond characterizations have been achieved using a combined experimental and theoretical charge density study. All intramolecular chemical bonds (N–N, C–N and C–H) of **atrz** molecule are typical covalent bonds. The relative bond strength is indicated according to the associated topological properties. The π-delocalization of the molecule is realized through Fermi hole distribution and MO analysis. The π-

delocalization of the molecule exists only on the triazole ring, the delocalization between two rings is blocked by a central localized *azo* double bond. The weak intermolecular hydrogen bonding and π-π interaction are illustrated; the donor/acceptor feature is clearly demonstrated through the density distribution and the molecular electrostatic potential. Such interactions are further manifested by the Hirshfeld surface.

Acknowledgements

We are grateful to generous support from National Science Council (now MOST) of Taiwan and to Computer and Information Networking Center of National Taiwan University for the support of high-performance computing facilities.

Notes and references

[a] Department of Chemistry, National Taiwan University, Taipei, Taiwan.
[b] Department of Chemistry, Soochow University, Taipei, Taiwan.
[c] Instrumentation Center, National Taiwan University, Taipei, Taiwan.
E-mail: wangyu@ntu.edu.tw; ccwang@scu.edu.tw

Electronic Supplementary Information (ESI) available: Twelve p_π-molecular orbitals of **atrz**, Crystal data and structure refinement for **atrz**, Agreement Indices of Various LS-Refinements for **atrz**, Thermal parameters (U_{ij}) and multipole populations (P_{lm}) of **atrz**, π−π interactions of **atrz** in crystal, H-bonds of **atrz**. See DOI: 10.1039/b000000x/

1. C. B. Aakeroy and K. R. Seddon, *Chem. Soc. Rev.*, 1993, **22**, 397; T. Kato and J. M. J. Fréchet, *Macromol. Symp.*, 1995, **98**, 311; C. M. Paleos and D. Tsiourvas, *Angew. Chem., Int. Ed.*, 1995, **34**, 1696; D. Braga and F. Grepioni, *Acc. Chem. Res.*, 2000, **33**, 601; L. Brammer, *Chem. Soc. Rev.*, 2004, **33**, 476.
2. G. A. Jeffrey and J. F. Piniella, *The Application of Charge Density Research to Chemistry and Drug Design*, Plenum Press, New York, 1991; V. G. Tsierelson and R. P. Ozerov, *Electron Density and Bonding in Crystals: Principles, Theory and X-ray Diffraction Experiments in Solid State Physics and Chemistry*, Institute of Physics Publishing, Bristol, U.K., 1996; P. Coppens, *X-ray Charge Densities and Chemical Bonding*, Oxford University Press, Oxford, 1997; P. Coppens, *Acta Crystallogr. Sect. A*, 1998, **54**, 779.
3. P. Coppens, *Angew. Chem., Int. Ed.*, 2005, **44**, 6810; T. S. Koritsanszky and P. Coppens, *Chem. Rev.*, 2001, **101**, 1583; C. Gatti, *Z. Kristallogr.*, 2005, **220**, 399.
4. E. Espinosa, E. Molins and C. Lecomte, *Chem. Phys. Lett.*, 1998, **285**, 170.
5. Y. A. Abramov, A. V. Volkov and P. Coppens, *Chem. Phys. Lett.*, 1999, **311**, 81; C. C. Wang, Y. Wang, H. J. Liu, K. J. Lin, L. K. Chou and K. S. Chan, *J. Phys. Chem. A*, 1997, **101**, 8887; C. R. Lee, C. C. Wang, K. C. Chen, G. H. Lee and Y. Wang, *J. Phys. Chem. A*, 1999, **103**, 156; M. R. V. Jorgensen, S. Cenedese, H. F. Clausen, J. Overgaard, Y. S. Chen, C. Gatti and B. B. Iversen, *Inorg. Chem.*, 2013, **52**, 297.
6. C. C. Wang, T. H. Tang and Y. Wang, *J. Phys. Chem. A*, 2000, **104**, 9566; C. R. Lee, L. Y. Tan and Y. Wang, *J. Phys. Chem. Solids*, 2001, **62**, 1613.
7. L.-C. Wu, C.-W. Hsu, Y.-C. Chuang, G.-H. Lee, Y.-C. Tsai and Y. Wang, *J. Phys. Chem. A*, 2011, **115**, 12602.
8. R. D. Poulsen, M. R. V. Jorgensen, J. Overgaard, F. K. Larsen, W. G. Morgenroth, T. Graber, Y. S. Chen and B. B. Iversen, *Chem. Eur. J.*, 2007, **13**, 9775; M. S. Schmokel, S. Cenedese, J. Overgaard, M. R. V. Jorgensen, Y. S. Chen, C. Gatti, D. Stalke and B. B. Iversen, *Inorg. Chem.*, 2012, **51**, 8607; M. S. Schmokel, L. Bjerg, J. Overgaard, F. K. Larsen, G. K. H. Madsen, K. Sugimoto, M. Takata and B. B. Iversen, *Angew. Chem., Int. Ed.*, 2013, **52**, 1503; S. Pillet, M. Souhassou, C. Mathoniere and C. Lecomte, *J. Am. Chem. Soc.*, 2004, **126**, 1219; N. Claiser, M. Souhassou, C. Lecomte, B. Gillon, C. Carbonera, A. Caneschi, A. Dei, D. Gatteschi, A. Bencini, Y. Pontillon and E. Lelievre-Berna, *J. Phys. Chem. B*, 2005, **109**, 2723.
9. R. F. W. Bader, *Atoms in Molecules: a Quantum Theory*, Clarendon Press, Oxford, 1990.
10. C. Gatti, R. Bianchi, R. Destro and F. Merati, *J. Mol. Struct. (THEOCHEM)*, 1992, **87**, 409; D. V. Fomitchev, T. R. Furlani and P. Coppens, *Inorg. Chem.*, 1998, **37**, 1519; L. J. Farrugia, P. R. Mallinson and B. Stewart, *Acta Crystallogr. Sect. B*, 2003, **59**, 234; L. J. Farrugia and C. Evans, *C. R. Chim.*, 2005, **8**, 1566; L. J. Farrugia and C. Evans, *J. Phys. Chem. A*, 2005, **109**, 8834.
11. E. Espinosa, I. Alkorta, J. Elguero and E. Molins, *J. Chem. Phys.*, 2002, **117**, 5529.
12. J. Overgaard and B. Iversen, in *Electron Density and Chemical Bonding I*, ed. D. Stalke, Springer, Berlin / Heidelberg2012, vol. 146, pp. 53; J. Overgaard, B. Schiott, F. K. Larsen, A. J. Schultz, J. C. MacDonald and B. B. Iversen, *Angew. Chem., Int. Ed.*, 1999, **38**, 1239; K. J. Lin, M. C. Cheng and Y. Wang, *J. Phys. Chem.*, 1994, **98**, 11685; C. R. Lee, C. C. Wang and Y. Wang, *Acta Crystallogr. Sect. B*, 1996, **52**, 966; P. Macchi, B. B. Iversen, A. Sironi, B. C. Chakoumakos and F. K. Larsen, *Angew. Chem., Int. Ed.*, 2000, **39**, 2719; Y. H. Mariam and R. N. Musin, *J. Phys. Chem. A*, 2008, **112**, 134; C. R. Lee, T. H. Tang, L. Chen and Y. Wang, *Chem. Eur. J.*, 2003, **9**, 3112.
13. E. Espinosa, C. Lecomte and E. Molins, *Chem. Phys. Lett.*, 1999, **300**, 745; C. C. Wang, T. H. Tang, L. C. Wu and Y. Wang, *Acta Crystallogr. Sect. A*, 2004, **60**, 488; P. Munshi and T. N. G. Row, *CrystEngComm*, 2005, **7**, 608; P. Munshi and T. N. G. Row, *J. Phys. Chem. A*, 2005, **109**, 659; P. Munshi and T. N. G. Row, *Acta Crystallogr. Sect. B*, 2006, **62**, 612; L. J. Farrugia, P. Kocovsky, H. M. Senn and S. Vyskocil, *Acta Crystallogr. Sect. B*, 2009, **65**, 757.
14. C. Gatti, E. May, R. Destro and F. Cargnoni, *J. Phys. Chem. A*, 2002, **106**, 2707; A. Ranganathan, G. U. Kulkarni and C. N. R. Rao, *J. Mol. Struct.*, 2003, **656**, 249; P. Munshi and T. N. Guru Row, *Crystallography Reviews*, 2005, **11**, 199.
15. M. Tonogaki, T. Kawata, S. Ohba, Y. Iwata and I. Shibuya, *Acta Crystallogr. Sect. B*, 1993, **49**, 1031; A. Puig-Molina, A. Alvarez-Larena, J. Piniella, S. Howard and F. Baert, *Struct. Chem.*, 1998, **9**, 395; R. S. Gopalan, P. Kumaradhas, G. U. Kulkarni and C. N. R. Rao, *J. Mol. Struct.*, 2000, **521**, 97; P. Coppens, Y. Abramov, M. Carducci, B. Korjov, I. Novozhilova, C. Alhambra and M. R. Pressprich, *J. Am. Chem. Soc.*, 1999, **121**, 2585; P. Macchi, A. J. Schultz, F. K. Larsen and B. B. Iversen, *J. Phys. Chem. A*, 2001, **105**, 9231; E. May, R. Destro and C. Gatti, *J. Am. Chem. Soc.*, 2001, **123**, 12248.
16. I. S. Konovalova, Y. V. Nelyubina, K. A. Lyssenko, B. V. Paponov and O. V. Shishkin, *J. Phys. Chem. A*, 2011, **115**, 8550.
17. Y.-C. Li, C. Qi, S.-H. Li, H.-J. Zhang, C.-H. Sun, Y.-Z. Yu and S.-P. Pang, *J. Am. Chem. Soc.*, 2010, **132**, 12172; Y. C. Chuang, C. T. Liu, C. F. Sheu, W. L. Ho, G. H. Lee, C. C. Wang and Y. Wang, *Inorg. Chem.*, 2012, **51**, 4663; Y. C. Chuang, W. L. Ho, C. F. Sheu, G. H. Lee and Y. Wang, *Chem. Commun.*, 2012, **48**, 10769.
18. C. Qi, S.-H. Li, Y.-C. Li, Y. Wang, X.-K. Chen and S.-P. Pang, *J. Mater. Chem.*, 2011, **21**, 3221.
19. N. K. Hansen and P. Coppens, *Acta Crystallogr. Sect. A*, 1978, **34**, 909.
20. A. Fischer, D. Tiana, W. Scherer, K. Batke, G. Eickerling, H. Svendsen, N. Bindzus and B. B. Iversen, *J. Phys. Chem. A*, 2011, **115**, 13061; K. Batke and G. Eickerling, *J. Phys. Chem. A*, 2013, **117**, 11566.
21. L. J. Farrugia and C. Evans, *C. R. Chim.*, 2005, **8**, 1566; L.-C. Wu, G.-H. Lee, C.-K. Chen and C.-C. Wang, *J. Chin. Chem. Soc. (Taipei, Taiwan)*, 2013, **60**, 823.
22. J. Overgaard, M. P. Waller, R. Piltz, J. A. Platts, P. Emseis, P. Leverett, P. A. Williams and D. E. Hibbs, *J. Phys. Chem. A*, 2007, **111**, 10123.
23. R. F. W. Bader, A. Streitwieser, A. Neuhaus, K. E. Laidig and P. Speers, *J. Am. Chem. Soc.*, 1996, **118**, 4959; R. J. Gillespie, I. Bytheway, T. H. Tang and R. F. W. Bader, *Inorg. Chem.*, 1996, **35**, 3954.
24. R. Ponec, G. Yuzhakov and R. Carbo-Dorca, *J. Comput. Chem.*, 2003, **24**, 1829; R. Ponec and F. Feixas, *J. Phys. Chem. A*, 2009, **113**, 8394.
25. Y. A. Abramov, *Acta Crystallogr. Sect. A*, 1997, **53**, 264.
26. S. Tsuzuki, K. Honda, T. Uchimaru, M. Mikami and K. Tanabe, *J. Am. Chem. Soc.*, 2002, **124**, 104; M. O. Sinnokrot and C. D. Sherrill, *J. Phys. Chem. A*, 2006, **110**, 10656.
27. D. Quinonero, A. Frontera, D. Escudero, P. Ballester, A. Costa and P. M. Deya, *Theor. Chem. Acc.*, 2008, **120**, 385.
28. S. Grimme, *Chem. Eur. J.*, 2004, **10**, 3423; K. Pluhackova, S. Grimme and P. Hobza, *J. Phys. Chem. A*, 2008, **112**, 12469; J. N. Latosinska, M. Latosinska, M. A. Tomczak, J. Seliger and V. Zagar, *J. Mol. Model*, 2011, **17**, 1781.

29. P. R. N. Kamya and H. M. Muchall, *J. Phys. Chem. A*, 2011, **115**, 12800.
30. M. P. Waller, A. Robertazzi, J. A. Platts, D. E. Hibbs and P. A. Williams, *J. Comput. Chem.*, 2006, **27**, 491.
31. J. J. McKinnon, D. Jayatilaka and M. A. Spackman, *Chem. Commun.*, 2007, 3814.
32. A. G. P. Maloney, P. A. Wood and S. Parsons, *CrystEngComm*, 2014, **16**, 3867.
33. , Nonius BV, Delft, The Netherlands.1998.
34. G. M. Sheldrick, Bruker AXS, Inc., Madison, WI2009.
35. G. M. Sheldrick, University of Gottingen1997.
36. T. Volkov, P. Macchi, L. J. Farrugia, C. Gatti, P. Mallinson, T. Richter and T. Koritsanszky, University of Buffalo, USA2006.
37. E. Clementi and C. Roetti., *Atomic Data and Nuclear Data Tables*, 1974, **14**, 177.
38. E. Clementi and D. L. Raimondi, *J. Chem. Phys.*, 1963, **38**, 2686.
39. *International Tables for X-ray Crystallography*, Kynoch Press: Birmingham1974.
40. T. Steiner, *Angew. Chem., Int. Ed.*, 2002, **41**, 48.
41. A. Volkov, T. Koritsanszky, M. Chodkiewicz and H. F. King, *J. Comput. Chem.*, 2009, **30**, 1379.
42. J. C. O. Alba and C. B. Jané, in *XAIM - X Atoms in Molecules Interface, version 1.0*, ver. 1.0 edn., 1998.
43. M. J. Frisch, G. W. Trucks, H. B. Schlegel, G. E. Scuseria, M. A. Robb, J. R. Cheeseman, G. Scalmani, V. Barone, B. Mennucci, G. A. Petersson, H. Nakatsuji, M. Caricato, X. Li, H. P. Hratchian, A. F. Izmaylov, J. Bloino, G. Zheng, J. L. Sonnenberg, M. Hada, M. Ehara, K. Toyota, R. Fukuda, J. Hasegawa, M. Ishida, T. Nakajima, Y. Honda, O. Kitao, H. Nakai, T. Vreven, J. Montgomery, J. E.; , J. E. Peralta, F. Ogliaro, M. Bearpark, J. J. Heyd, E. Brothers, K. N. Kudin, V. N. Staroverov, R. Kobayashi, J. Normand, K. Raghavachari, A. Rendell, J. C. Burant, S. S. Iyengar, J. Tomasi, M. Cossi, N. Rega, J. M. Millam, M. Klene, J. E. Knox, J. B. Cross, V. Bakken, C. Adamo, J. Jaramillo, R. Gomperts, R. E. Stratmann, O. Yazyev, A. J. Austin, R. Cammi, C. O. Pomelli, J. W.; , R. L. Martin, K. Morokuma, V. G. Zakrzewski, G. A. Voth, P. Salvador, J. J. Dannenberg, S. Dapprich, A. D. Daniels, Ö. Farkas, J. B. Foresman, J. V. Ortiz, J. Cioslowski and D. J. Fox, in *Gaussian 09, Revision B.01; Gaussian, Inc. Wallingford CT*, Gaussian, Inc., Wallingford CT, Revision B.01 edn., 2009.
44. J. D. Chai and M. Head-Gordon, *Phys. Chem. Chem. Phys.*, 2008, **10**, 6615.
45. M. A. Spackman and J. J. McKinnon, *CrystEngComm*, 2002, **4**, 378; J. J. McKinnon, M. A. Spackman and A. S. Mitchell, *Acta Crystallogr. Sect. B*, 2004, **60**, 627.
46. S. K. Wolff, D. J. Grimwood, J. J. McKinnon, D. Jayatilaka and M. A. Spackman, University of Western Australia, Ver. 1.5 edn., 2005.

